Thermochimica Acta 495 (2009) 129–138

Contents lists available at ScienceDirect

Thermochimica Acta

journal homepage: www.elsevier.com/locate/tca

The non-isothermal thermogravimetric tests of animal bones combustion. Part. I. Kinetic analysis

Bojan Janković [a,*], Ljiljana Kolar-Anić [a], Ivana Smičiklas [b], Slavko Dimović [b], Dragana Arandelović [c]

[a] Faculty of Physical Chemistry, University of Belgrade, Studentski trg 12-16, P.O. Box 137, 11001 Belgrade, Serbia
[b] Vinča Institute of Nuclear Sciences, Mike Petrovića Alasa, P.O. Box 522, 11001 Belgrade, Serbia
[c] Institute of General and Physical Chemistry, Studentski trg 12-16, 11001 Belgrade, Serbia

ARTICLE INFO

Article history:
Received 11 February 2009
Received in revised form 6 June 2009
Accepted 10 June 2009
Available online 18 June 2009

Keywords:
Bone
Combustion
Differential thermal analysis
Thermogravimetric analysis
Kinetic analysis
Autocatalytic

ABSTRACT

The non-isothermal combustion of animal bones was investigated by simultaneous thermogravimetric and differential thermal analysis (TG–DTA), in the temperature range ΔT = 20–650 °C. The full kinetic triplet (A, E_a and $f(\alpha)$) for the investigated process was established, using different calculation procedures: isoconversional (model-free) and the Kissinger's methods. The non-isothermal process occured through three reaction stages (I, II and III). Stage I was described by a reaction model, which contains two competing reactions with different values of the apparent activation energy. The autocatalytic two-parameter Šesták–Berggren (SB) model (conversion function $f(\alpha) = \alpha^{0.62}(1-\alpha)^{3.22}$), best described the second (II) reaction stage of bone samples. This stage, which corresponds to the degradation process of organic components (mainly collagen), exhibited the autocatalytic branching effect, with increasing complexity. Stage III, attributed to the combustion process of organic components, was best described by an n-th reaction order model with parameter $n = 1.5$ ($f(\alpha) = (1-\alpha)^{1.5}$). The appearance of compensation effect clearly showed the existence of three characteristic branches attributed to the dehydration, degradation and combustion processes, respectively, without noticable changes in mineral phase. The isothermal predictions of bone combustion process, at four different temperatures (T_{iso} = 200, 300, 400 and 450 °C) were established in this paper. It was concluded that the shapes of the isothermal conversion curves at lower temperatures (200–300 °C) were similar, whereas became more complex with further temperature increase due to organic phase degradation.

1. Introduction

Bone is a complex composite material consisting of approximately 10% water, 30% organic phase (mainly collagen fibrils) and 60% inorganic material (predominantly carbonated hydroxyapatite) [1]. It serves a number of functions, such as providing the cells found in the marrow that differentiate into blood cells, and also acting as a calcium reservoir. Nevertheless, its primary purpose is to provide mechanical support for soft tissues and serve as an anchor for the muscles that generate motion [2]. Materials derived from bone have potential for applications in many areas spanning the biomedical [3–6], environmental [7,8] and industrial [9,10] fields. A range of experimental techniques have been employed in the studies of bones and bone derived materials, including scanning electron microscopy (SEM) [11–13], X-ray diffraction (XRD) [14–16], and infrared spectroscopy (IR) [17–20], as well as the thermal analysis (TG/DTA) [21,22].

Thermal analysis can provide valuable information regarding the organic and mineral content of bones. Thermal methods have been applied for the characterization of bones from various species [23–25], dating of archaeological samples [21] and for the characterization of both the organic and inorganic phases for the development of synthetic analogues [26]. However, although thermal analysis methods can also be useful for obtaining informations about reaction kinetics [27,28], they were seldom used to describe kinetics of bone samples combustion.

In the literature, information about the estimated values of combustion kinetic parameters can be found for different bone like materials. The effect of bone char initial surface area and heating rate on the production of carbon-free bone ash was investigated [29], as well as kinetics of meat and bone meal products (MBM) thermal degradation [30–35] since co-firing with coal in combustion plants represent a promising way of MBM disposal. However, the composition of both bone char and MBM differ significantly in comparison to raw powdered animal bone, for which complete kinetic analysis was not found.

* Corresponding author. Faculty of Physical Chemistry, Department of Dynamics and Matters Structure, University of Belgrade, Studentski trg 12-16, P.O. Box 137, 11001 Belgrade, Serbia. Tel.: +381 11 2187 133; fax.: +381 11 2187 133.
E-mail address: bojanjan@ffh.bg.ac.rs (B. Janković).

0040-6031/$ – see front matter © 2009 Elsevier B.V. All rights reserved.
doi:10.1016/j.tca.2009.06.016

Generally, the main reasons for measuring rates of reactions are to obtain information about the reaction mechanism, which may prove useful in modifying the course of the reaction, predicting the behavior of similar reactions, and/or in kinetic parameters determination which may allow determination of reaction rates under different conditions by interpolation or extrapolation [36]. The reaction mechanism, can usually only be inferred from the overall picture constructed from the results of the mathematical side of kinetic analysis (determination of the kinetic (reaction) model) and as much complementary evidence (e.g., spectroscopy, chemical and structural analysis, etc.) as possible.

The major goal of the present work was the investigation of kinetic properties of the animal (beef) bones non-isothermal combustion processes. From the obtained experimental data full kinetic triplet (pre-exponential factor (A), the apparent activation energy (E_a) and analytical form of reaction model function, $f(\alpha)$ or $g(\alpha)$) were established. Furthermore, the kinetic triplet was estimated using the isoconversional (Friedman (FR) [37], Flynn–Wall–Ozawa (FWO) [38,39] and Kissinger–Akahira–Sunose (KAS) [40,41]) and the Kissinger's [40] methods in combination with the composite differential method I [42] and differential master plot method [42,43].

2. Materials and methods

2.1. Bone sample

The sample used in this study originated from bovine (femur) bones. Bones were cleaned from meat, cut into smaller pieces, boiled in distilled water in order to remove fat and subsequently dried in the oven at 80 °C. Fraction of particle size 45–200 μm, obtained by milling and sieving, was used for the TG–DTA measurements. The details about sample preparation and characterization are published elsewhere [44].

2.2. Thermal measurements

Simultaneous differential thermal analysis (DTA) and thermogravimetric analysis (TGA) were performed on STA-1000 Simultaneous Thermal Analyzer, Stanton Redcroft, UK. The bone samples with approximately $m \approx 5$–10 mg were heated at three different heating rates $\beta = 2.5, 5$ and 20 °C min^{-1}, in air atmosphere (air flow $\varphi = 20$ ml min^{-1}) in the temperature range of $\Delta T = 20$–650 °C.

3. Kinetic analysis

Kinetic analysis of combustion process is traditionally expected to produce an adequate kinetic description of the process in terms of the reaction model and of the Arrhenius parameters using a single-step kinetic equation in the following form:

$$\frac{d\alpha}{dt} = k(T)f(\alpha) \tag{1}$$

where t is the time, T is the temperature, α is the extent of conversion (for a gravimetric measurement, α is defined by $\alpha = (m_o - m_t)/(m_o - m_f)$ where, m_o is the initial mass, m_t is the mass at time t (or temperature T) and m_f is the final mass) and $f(\alpha)$ is the function of reaction model. The temperature dependence of the rate constant is introduced by replacing $k(T)$ with the Arrhenius equation, which gives

$$\frac{d\alpha}{dt} = A\exp\left(-\frac{E_a}{RT}\right)f(\alpha) \tag{2}$$

where A (the pre-exponential factor) and E_a (the apparent activation energy) are the Arrhenius parameters and R is the gas constant.

If the temperature of the sample is changed by a controlled and constant heating rate, $\beta = dT/dt$, the variation in the extent of conversion can be analyzed as a function of temperature, this temperature being dependent on the time of heating. Therefore, the rearrangement of Eq. (2) gives

$$\beta\frac{d\alpha}{dT} = A\exp\left(-\frac{E_a}{RT}\right)f(\alpha). \tag{3}$$

As the studied compounds have complex structures, it can be hypothesised that several steps with different energies will be involved. If a process involves several steps with different apparent activation energies, the relative contributions of these steps to the overall reaction rate will vary with both temperature and the extent of conversion. This means that the effective activation energy, determined from the analysis of the results, will also be a function of these two variables.

An alternative approach to kinetic analysis is the model-free methods that allow for evaluating the Arrhenius parameters without choosing the reaction model. The isoconversional methods make up the best representation of the model-free approach.

These methods yield the variation of the effective activation energy as a function of the extent of conversion (α). The knowledge of the dependence E_a on α allows detecting multi-step processes and predicting the reaction kinetics over a wide temperature range. The efficacy of the isoconversional analysis originates from its ability of disclosing and handling the complexity of the respective processes. As a matter of fact, the isoconversional analysis provides a fortunate compromise between the oversimplified but widely used single-step Arrhenius kinetic treatments and the prevalent occurrence of processes whose kinetics are multi-step and/or non-Arrhenius [45].

3.1. Isoconversional (model-free) methods

The differential isoconversional method suggested by Friedman (FR) [37] is based on Eq. (3) that leads to:

$$\ln\left[\beta_i\left(\frac{d\alpha}{dT}\right)\right] = \ln[Af(\alpha)] - \frac{E_a}{RT_\alpha} \tag{4}$$

where T_α is the temperature at which the system approach a conversion α, and β_i is the actual heating rate. For a constant α, a plot of $\ln[\beta_i(d\alpha/dT)]$ versus $1/T_\alpha$ should be a straight line whose slope allows the calculation of the apparent activation energy.

The integral isoconversional methods are based on the integration of Eq. (3):

$$g(\alpha) = \frac{A}{\beta}\int_0^T \exp\left(-\frac{E_a}{RT}\right)dT = \frac{AE_a}{\beta R}p(x) \tag{5}$$

where $x = E_a/RT$ and $p(x)$ is the so-called temperature or exponential integral which cannot be exactly calculated [46,47]. Actually, integral methods differ depending on the approximation of this integral. One of them is that given by Flynn and Wall [38] and Ozawa [39], which relies on Doyle approximation [48]:

$$\ln p(x) = -5.331 - 1.052x \tag{6}$$

Taking logarithms in Eq. (5) and substituting in Eq. (6) we have:

$$\ln\beta = \ln\frac{AE_a}{Rg(\alpha)} - 5.331 - 1.052\frac{E_a}{RT} \tag{7}$$

For a constant conversion, a plot of $\ln\beta$ versus $1/T$, from the data at the different heating rates, leads to a straight line whose slope provides E_a calculation. This method is known as Flynn–Wall–Ozawa (FWO) method.

In the Kissinger–Akahira–Sunose method (KAS) [40,41], the expression $p(x)$ is expressed using the Coats–Redfern approxima-

tion [49]:

$$p(x) \cong \frac{\exp(-x)}{x^2} \tag{8}$$

Substituting this into Eq. (5) and taking logarithms we obtain:

$$\ln\left(\frac{\beta}{T^2}\right) \cong \ln\left(\frac{AR}{E_a g(\alpha)}\right) - \frac{E_a}{RT} \tag{9}$$

A plot of $\ln(\beta/T^2)$ versus $1/T$ for a constant conversion gives the E_a at that conversion.

3.2. Kissinger (peak) method

Kissinger's method assumes that the reaction rate has maximum value at the peak temperature (T_p) [40]. This assumption also implies a constant extent of conversion (α) at T_p. In many cases, the extent of conversion (α_p) at T_p varies with the heating rate and hence raises doubt about grouping this method into isoconversional category. The Kissinger's equation [40] can be presented in the following form:

$$\ln\left(\frac{\beta}{T_p^2}\right) = \ln\left(\frac{AR}{E_a}\right) - \frac{E_a}{RT_p} \tag{10}$$

This method provides the value of A apart from the value of the apparent activation energy E_a. Here one gets single value of E_a using Eq. (10).

3.3. Composite differential method I

The composite methods presuppose one single set of Arrhenius parameters for all conversions and heating rates. In this way all the experimental data can be superimposed in one single master curve.

Composite differential method I [42] is based directly on Eq. (3) and can be presented in the following form:

$$\ln\left[\frac{\beta(\mathrm{d}\alpha/\mathrm{d}T)}{f(\alpha)}\right] = \ln A - \frac{E_a}{RT} \tag{11}$$

For each form of $f(\alpha)$, the curve $\ln[\beta(\mathrm{d}\alpha/\mathrm{d}T)/f(\alpha)]$ versus $1/T$ was plotted for the experimental data obtained at the different heating rates. We then chose the kinetic model for which the data falls in a single master straight line and which gives the best linear correlation coefficient. A single set of Arrhenius parameters, E_a and A, can be obtained from the slope and the intercept of the straight line.

The commonly used differential ($f(\alpha)$) and integral ($g(\alpha)$) expressions for different reaction models are applied in this work [50,51].

3.4. Differential master plot method

Once the apparent activation energy has been determined it is possible to find the kinetic model which corresponds to the better description of the experimental data issued from the TG experiments. Using as a reference point at $\alpha = 0.5$, the following differential master equation is easily derived from Eq. (3) [42,43]:

$$\frac{f(\alpha)}{f(0.5)} = \frac{(\mathrm{d}\alpha/\mathrm{d}t)}{(\mathrm{d}\alpha/\mathrm{d}t)_{0.5}} \frac{\exp(E_a/RT)}{\exp(E_a/RT_{0.5})} \tag{12}$$

where $(\mathrm{d}\alpha/\mathrm{d}t)_{0.5}$, $T_{0.5}$ and $f(0.5)$ are, respectively, the reaction rate, the temperature reaction and the differential function of reaction model at $\alpha = 0.5$.

The left hand-side of Eq. (12) is a reduced theoretical curve which is characteristic of each kinetic function. The right hand-side of the equation is associated with the reduced rate and can be obtained from experimental data if the apparent activation energy is known. Comparison of both sides of Eq. (12) tells us which kinetic model describes an experimental reaction process.

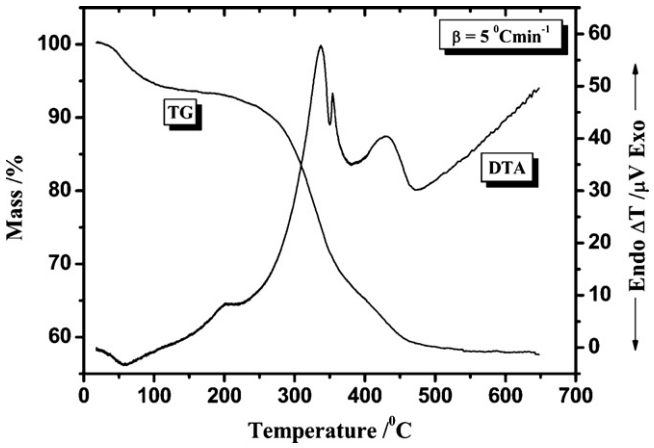

Fig. 1. TG and DTA curve for the combustion process of bovine bone sample in an air atmosphere recorded at $\beta = 5\,^{\circ}\mathrm{C\,min^{-1}}$.

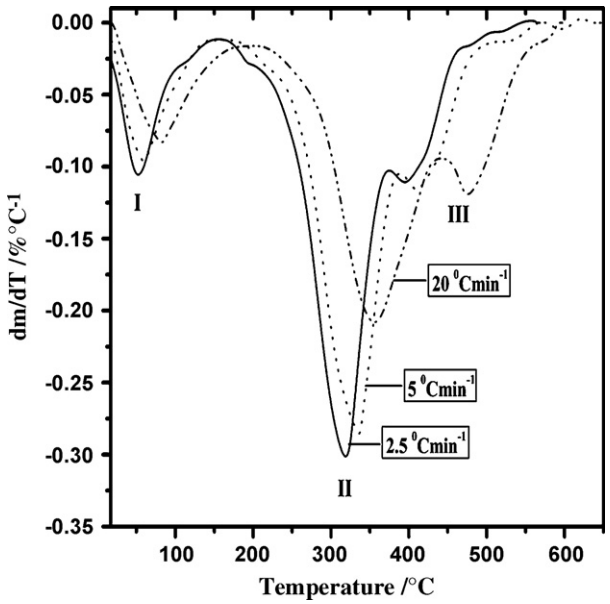

Fig. 2. DTG curves for the combustion process of bovine bone samples in an air atmosphere recorded at the different heating rates ($\beta = 2.5$, 5 and $20\,^{\circ}\mathrm{C\,min^{-1}}$).

4. Results

From the characterization approach, the X-ray diffraction (XRD) analysis of investigated bone sample confirmed that the hydroxyapatite (HAP) is the major crystalline phase present [44]. The bands characteristic for carbonate substituted HAP were also detected in IR spectra, with the addition of amide I, II and III bands and bands characteristic for $-CH_2$, carbonyl group and hydrogen-bonded H_2O molecules [44]. The specific surface area of the bone sample was found to be rather small $0.1\,\mathrm{m^2\,g^{-1}}$ [44], which is in accordance with dense bone structure built up from nanosized HAP crystals and collagen fibers.

As expected, the combustion of animal bones under non-isothermal conditions is a rather complicated process especially due to the various kinds of molecules which are present in the investigated samples.

Fig. 1 shows the example of TG–DTA curves, recorded in air atmosphere, for the investigated sample of animal bones at $\beta = 5\,^{\circ}\mathrm{C\,min^{-1}}$, whereas Fig. 2 represents the DTG curves at all considered heating rates ($\beta = 2.5$, 5 and $20\,^{\circ}\mathrm{C\,min^{-1}}$).

Table 1
The parameters of the reaction steps for bovine bone samples heated at the different heating rates (2.5, 5 and 20 °C min^{-1}).

Stage	β (°C min^{-1})	Data from TG–DTA curves						Data from TG–DTG curves					
		T_i (°C)[a]	T_f (°C)[a]	Δm_t (%)[b]	$<\Delta m_t>$ (%)[c]	T_p (°C)[d]	m_p (%)[e]	T_i (°C)[a]	T_f (°C)[a]	Δm_t (%)[b]	$<\Delta m_t>$ (%)[c]	T_p (°C)[d]	m_p (%)[e]
I	2.5	18.1	190.9	7.1	7.5	50.6	2.0	18.1	188.2	7.0	7.4	49.9	1.9
	5	19.1	203.0	7.0		57.8	2.3	19.1	201.4	6.9		56.6	2.2
	20	19.5	232.7	8.4		83.1	3.6	19.5	226.1	8.3		82.9	3.5
II	2.5	190.9	361.2	25.2	24.8	320.8	16.8	188.2	365.9	25.5	25.4	319.8	16.6
	5	203.0	377.7	25.5		337.4	17.7	201.4	382.3	26.1		336.2	17.6
	20	232.7	426.9	23.8		388.0	18.6	226.1	435.0	24.5		359.3	13.6
III	2.5	361.2	563.2	8.7	9.6	419.8	5.8	365.9	563.2	8.3	9.0	397.1	3.1
	5	377.7	633.5	9.5		429.5	5.3	382.3	633.5	9.0		413.5	3.0
	20	426.9	594.6	10.5		476.1	4.8	435.0	594.6	9.7		474.4	3.7

[a] T_i and T_f—temperatures at the beginning and at the end of each reaction step, according to DTA or DTG curves, respectively.
[b] Δm_t—the total mass loss corresponding to each step.
[c] $\langle\Delta m_t\rangle$—average value of Δm_t values.
[d] T_p—the peak temperature corresponding to the "maximum" in DTA or DTG curve.
[e] m_p—the total mass loss from the beginning of heating until the maximum rate of the considered step.

The inspection of DTA curve for the bone sample shows one endothermic peak in the temperature range of approximately ΔT = 20–125 °C and several exothermic peaks in the temperature range ΔT = 175–500 °C. The first of these peaks is a small, with maxima at 190–230 °C. The second exothermic peak is a complex one with two distinctive maxima. The third broad peak appears in the temperature range of approximately ΔT = 400–480 °C. The DTG curves for bone samples clearly show three groups of peaks with different intensities which corresponds to the considered reaction steps (steps I, II and III) (Fig. 2).

The main parameters of the above-mentioned steps for the investigated system are listed in Table 1.

Comparing the thermal combustion data of bone samples (Table 1), it can be noticed that the most significant difference is related to the stages II and III, concerning the values of T_i, T_f, Δm_t, $\langle m_t\rangle$ and T_p.

From Fig. 1, it can be seen that the bone sample lost mass up to 210 °C when heated in air atmosphere. This mass loss was associated with loss of water (stage I, Table 1). In addition to bone mineral and organic matrix, water is an abundant component of bone, accounting for up to 10% by weight. Much of this water occurs in the pore spaces between the mineral phosphate surface and the collagen, responsible for nutrient diffusion and contributing to the viscoelastic properties of the material. Fig. 1 shows mass loss in the temperature range from 210 to 380 °C in air. In this range, mass loss can be associated primary with thermal decomposition of organic phase (stage II, Table 1). It can be pointed out, that in this stage, the loss of bulk water can be followed by deeper dehydration, with the loss of the ordered hydration shell that has been proposed to mediate the interactions between the mineral and collagen components of bone [52]. Also, it can be pointed out, that the high organic content samples usually lost carbon dioxide in two stages [53]. In an oxidizing atmosphere the organic phase is expected to be removed up to 600 °C [23].

4.1. Model-free analysis

The dependence of the apparent activation energy (E_a) values on the extent of conversion (α) for the investigated process was evaluated from the straight line slope of the correspondent FR (Eq. (4)), KAS (Eq. (9)) and FWO (Eq. (7)) isoconversional methods. The results obtained for bone combustion process are shown in Fig. 3.

In presented figure, we can observe a strong dependence of E_a values on α for considered bone sample. E_a values determined by means of integral isoconversional methods ($E_{a,\mathrm{KAS}}$ (□) and $E_{a,\mathrm{FWO}}$ (○)) are in good agreement, but they are different from that determined by Friedman differential method (($E_{a,\mathrm{FR}}$) (■)). It has been shown that the existence of significant differences between $E_{a,\mathrm{FR}}$ and E_a calculated using all integral isoconversional methods are due to the way of deriving the relations, which ground the integral methods. These relations are derived considering that the activation parameters do not depend on the extent of conversion. Obviously, if E_a and A depend on the extent of conversion (α), these derivations are not correct. Therefore, in such cases, the Friedman (FR) method, which uses directly the equation of reaction rate, is recommended [54]. The susceptibility of the Friedman (FR) method to errors arising from experimental noise can be effectively mitigated if the rate of data recording during experiments is high so that the raw data can be significantly smoothed prior to the application of the derivative-based Friedman technique. So with proper smoothing of the data, the Friedman technique seems to be a reliable technique in all cases. Among the two integral isoconversional methods used in this work, the kinetic measurements and predictions from the KAS method seem to be much more accurate than the FWO method (which includes a very crude approximation of the temperature integral $p(x)$ in Eq. (5)), but less accurate than the derivative-based Friedman (FR) method.

From Fig. 3, for three reaction steps of bone sample, the following dependencies of $E_{a,\ \mathrm{FR}}$ on α can be observed:

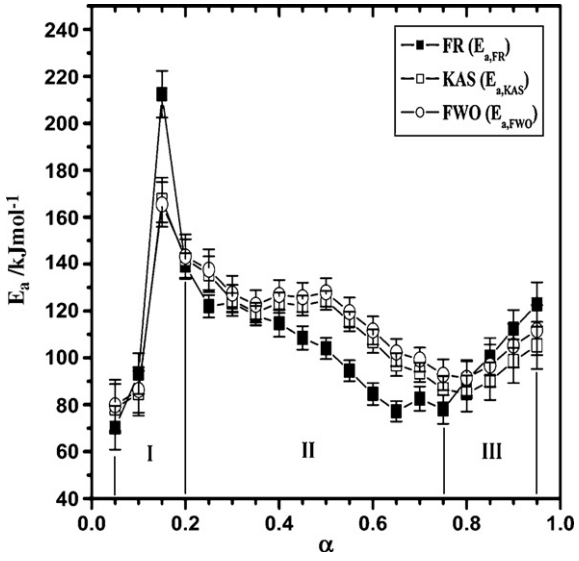

Fig. 3. Dependence of the apparent activation energy (E_a) on the extent of conversion (α) evaluated from the FR, KAS and FWO methods, for combustion process of bovine bone sample (reaction steps are designated as I, II and III).

(a) For step I, $E_{a,\ FR}$ abruptly increases from 70.2 ± 9.3 kJ mol^{-1} (for $\alpha = 5\%$) to 212.4 ± 9.9 kJ mol^{-1} (for $\alpha = 15\%$). These results show that the water molecules are strongly bounded in bone structure, and in such a manner the higher value of E_a is needed for the liberation of water. In order to get a better insight in water binding with different structural components of bone, it is necessary to perform a detailed spectroscopic study (for example, the nuclear magnetic resonance (NMR) measurements) [55–57]. However, in accordance with the available literature [55,56], we may suppose that the obtained values of E_a in the range $70.2 \leq E_{a,FR} \leq 93.3$ kJ mol^{-1} can be attributed to the liberation energy of bulk water which fills the pores of the calcified matrix. It can be pointed out, that these values of E_a are much higher than values of E_a needed for pure desorption of water molecules from bone surface. The relatively wide range of the apparent activation energies ($E_{a,FR} = 70.2$–93.3 kJ mol^{-1}) can be probably attributed to the existence of pore size distribution in our investigated bone sample. In addition, with increasing of T and α, the higher value of E_a ($E_{a,FR} = 212.4$ kJmol^{-1} for $\alpha = 15\%$) is needed for the liberation of structural water molecules tightly bound to bone components. These water molecules probably occupy the vacancies created by substitutions and defects in the crystal lattice of apatite structure. Furthermore, the role of mentioned water molecules is probably stabilizing the local structure forming the hydrogen-bonding bridges between surrounding ions [58–60]. Hydrogen-bonded water-bridges also have role of stabilizing the collagen triple helix [58], consequently the higher value of E_a is necessary.

(b) For step II, $E_{a,FR}$ decreases from 139.4 ± 5.2 kJ mol^{-1} (for $\alpha = 20\%$) to 78.0 ± 6.1 kJ mol^{-1} (for $\alpha = 75\%$). This step represents the progressive decomposition of organic components, mainly collagen structure.

(c) For step III, $E_{a,FR}$ almost linearly increases from 90.7 ± 7.8 kJ mol^{-1} (for $\alpha \approx 78\%$) to 122.8 ± 9.4 kJ mol^{-1} (for $\alpha = 95\%$). The mineral content was derived from the mass remaining at about 600 °C, after all the organic material had been removed. It can be pointed out, that since there was no loss of mass beyond 600 °C, it was assumed that the remaining mass consists only of HAP and of no organic matter. At temperatures greater than 600 °C, combustion of carbonate may occur. In our previous study, a small weight loss (1.88%) observed in the temperature range 640–900 °C, without notable peak in the DTA curve, was attributed to the carbonates combustion [44]. This process, however, was not observed in experimentally obtained TG–DTA–DTG curves presented in this study, as the experiments were conducted up to 600 °C.

The additionally explanation connected with the above-mentioned reaction step can be obtained by further kinetic analysis. From the above strong α dependence of E_a values shows that all reaction steps of bone sample exhibit complex mechanisms.

According to Vyazovkin and Sbirrazzuoli [61] a generalized linear relationship can be established between pre-exponential factor and apparent activation energy as:

$$\ln A_\xi \cong a + bE_{a,\xi} \tag{13}$$

where a and b are constant parameters or compensation coefficients.

This relationship has been known as the compensation effect. The compensation effect can be used to find out whether the variations of apparent activation energy with different factors (ξ), which produce a change in the kinetic parameters, has a physical back ground or they are caused by variations of process conditions or calculation manipulation. According to Eq. (4), the constant $\ln[Af(\alpha)]$ can be determined from the intercept of each isoconversional line.

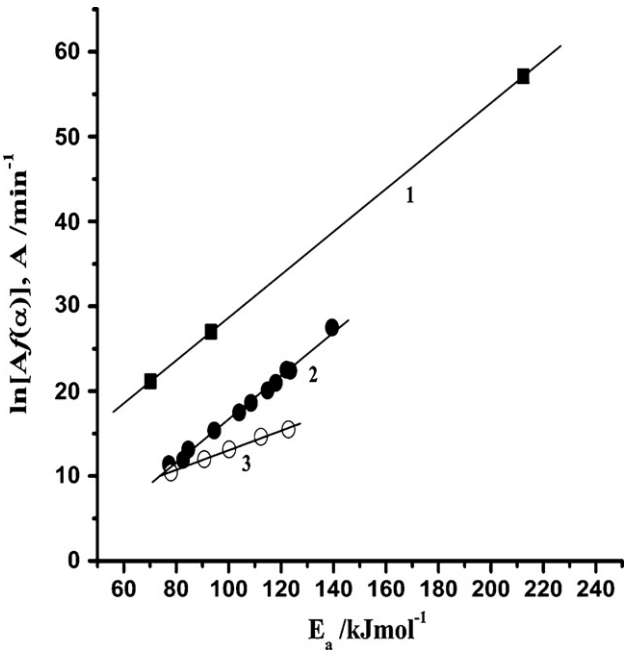

Fig. 4. The plots of $\ln[Af(\alpha)]$ versus apparent activation energy (E_a) at the different extent of conversion for the investigated combustion process (three characteristically reaction branches (I, II and III) are presented in the same figure).

The plots of $\ln[Af(\alpha)]$ versus E_a for the investigated process are shown in Fig. 4.

The presented plots show three different processes, at the start, at the middle and at the last part of the reaction (three branches), respectively. It can be deduced that the non-isothermal animal bones combustion in air atmosphere divided into three distinctive areas in the term of the extent of conversion. It can be seen from the established plots, that the first branch [(1)] is completely independent from other two branches (branches [(2)] and [(3)]) (Fig. 4). The trend lines marked with (■), (●) and (○) are related to the conversions lower than 0.15, conversion values in range 0.20–0.75 and conversion values higher than 0.75, respectively.

The values of intercept (a), slope (b) and linear correlation coefficient (r) related to the above linear curves are listed in Table 2.

The difference between parameter values (a, b) for these lines, implies that the investigated process at lower, medial and upper values of conversion follows different routes. In fact, Fig. 4 and the results which are listed in Table 2, suggest three different processes, at the beginning, in the middle, and at the end of the reaction. It can be observed that the processes described by the branches [(2)] and [(3)] are linked and mutually dependent.

Table 3 shows the values of kinetic parameters calculated by the Kissinger's peak method for the investigated process in air atmosphere.

It can be seen from Table 3 that E_a value calculated by Kissinger's method is lower and higher than corresponded values of E_a obtained by the Friedman's isoconversional method for regions I

Table 2
The values of intercept (a), slope (b) and linear correlation coefficient (r) of the trend lines related to the branches 1, 2 and 3, for corresponding reaction steps of bovine bone samples.

Branch	Bovine bone		
	a/min^{-1}	b/mol kJ^{-1}	r
1	3.3898	0.2529	1.0000
2	−8.8494	0.2555	0.9970
3	1.5158	0.1652	0.9977

Table 3
The values of kinetic parameters (E_a, A) calculated by the Kissinger's (peak) method, for the considered reaction steps (peaks I, II and III) of bovine bone samples.

Method	E_a (kJ mol^{-1})			A/min^{-1}		
	Peak I	Peak II	Peak III	Peak I	Peak II	Peak III
Kissinger	53.7 ± 0.7	88.6 ± 0.9	138.6 ± 1.9	7.86×10^7	2.74×10^8	2.85×10^9

and III, respectively (Fig. 3). For region II, the value of E_a calculated by the Kissinger's method is in good agreement with values of E_a calculated by the Friedman's method at approximately $\alpha = 0.55$.

4.2. Determination of reaction mechanism

To calculate the pre-exponential factor from the apparent activation energy obtained from the isoconversional procedure (FR, KAS or FWO method), firstly we determined the kinetic model which better fits with the experimental results. We used the composite differential method I and the differential master plot method. For kinetic model derivation, we used several proposed theoretical reaction mechanisms like n-th reaction order, autocatalytic, diffusion, nucleation (Avrami-Erofeev) and contraction. These models have not been described here because they are widely documented in the literature [50,51].

The kinetic model which best describe the complex combustion process is searched for stages II and III. Because of existing the very large variation of E_a on α (from 70.2 to 212.4 kJ mol^{-1}) in the first reaction stage, the determination of kinetic model can be unreliable, since in that case the calculated values of E_a and A, do not represent the real values of kinetic parameters.

By introducing the various analytical forms of $f(\alpha)$ functions for analyzed kinetic models [50,51] in Eq. (11) at all considered heating rates, we selected an autocatalytic two-parameter Šesták–Berggren (SB) [62] model $f(\alpha) = \alpha^{0.62}(1-\alpha)^{3.22}$ for the second stage of bone combustion process.

Fig. 5 shows how all the data for the SB reaction model with parameters $m = 0.62$ and $n = 3.22$ (full square (■) symbol) fits onto just one master straight line, for the second combustion stage of bone sample. It can be seen that large deviations from the single master curve do not exist.

Furthermore, the overall differential kinetic parameters (E_a, A) for this model ($E_a = 91.8 \pm 0.3$ kJ mol^{-1}, ln$A = 17.68$ (A in min^{-1}), $r = -0.9918$) are similar to the values of kinetic parameters obtained by the Kissinger's method (Table 3). Criado et al. [42] demonstrate that for the thermal decomposition of solid samples, composite methods allow us to differentiate between models that can correctly reproduce the thermal process despite having different kinetic parameters. According to these authors, the model in which the data are grouped together in just one straight line (Eq. (11)) is the correct one and the kinetic parameters obtained from this straight line are the real ones.

In order to confirm the established kinetic model for the second reaction stage, we used the differential master curves. Fig. 6 shows the theoretical and experimental differential curves established using Eq. (12). The experimental curves are shown for calculated overall apparent activation energy from composite differential method I.

It can be seen that the experimental master curves at considered heating rates fits very well the theoretical master curves for the SB model with increasing trend of both kinetics exponents (m and n). The values of SB parameters calculated from the composite differential method I ($m = 0.62$; $n = 3.22$) represent the average values of SB parameters obtained from the differential master curves at different heating rates.

Furthermore, by introducing the various analytical forms of $f(\alpha)$ functions [50,51] in Eq. (11) at all considered heating rates, we selected an n-th reaction order model with $n = 1.5$ ($f(\alpha) = (1-\alpha)^{1.5}$) for third reaction stage.

Fig. 5 shows how all the data for the $n = 1.5$ models (full circle (●) symbol) fits onto just one master straight line, for third stage of combustion process. It can be seen from Fig. 5 that all points are placed around/on the same line only for $n = 1.5$.

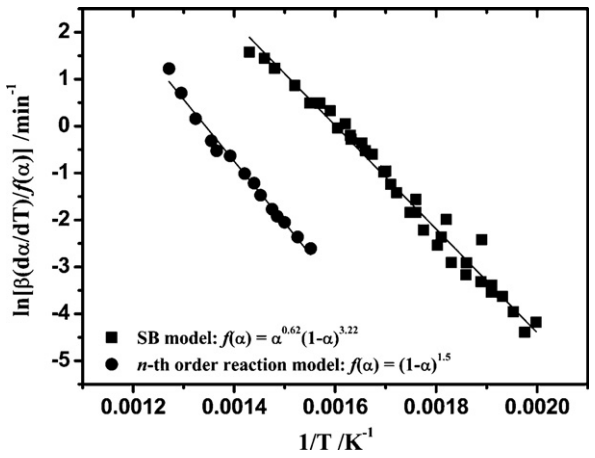

Fig. 5. Composite differential method analysis of non-isothermal TG data (2.5, 5 and 20 °C min^{-1}) based on Eq. (11) for the second (II) and the third (III) reaction stage. The filled symbols correspond to the differential data, for SB reaction model with $m = 0.62$ and $n = 3.22$ (symbol (■)) and n-th order reaction model with $n = 1.5$ (F1.5) (symbol (●)).

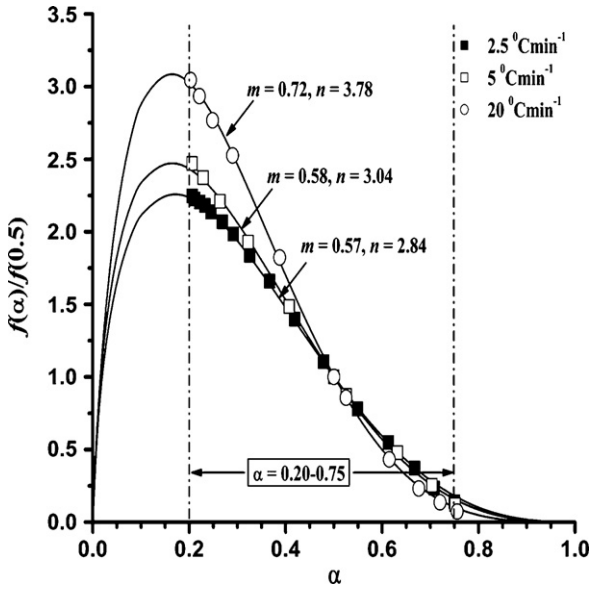

Fig. 6. A comparison of the theoretical differential master plots of $f(\alpha)/f(0.5)$ versus α (full lines) with the experimental master curve at the considered heating rate, for the second (II) reaction stage of bovine bone samples. The symbols correspond to experimental data determined using Eq. (12), with value of the apparent activation energy obtained from composite differential method.

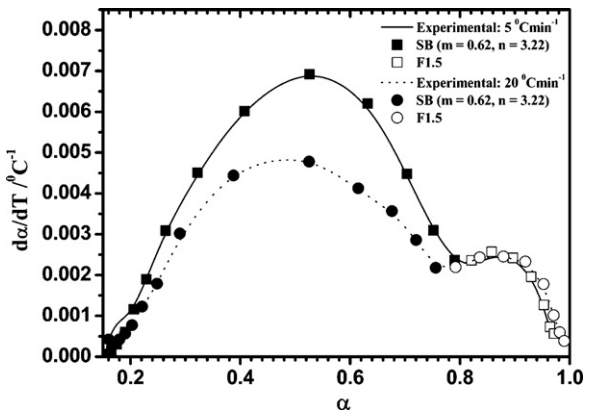

Fig. 7. The experimental and simulated reaction rate versus the extent of conversion at $\beta = 5\,^{\circ}\mathrm{C\,min^{-1}}$ and $20\,^{\circ}\mathrm{C\,min^{-1}}$, for the second (II) and third (III) reaction stages. The continuous (full and dash) lines represent the experimental data. The full and empty symbols represent the simulated data using Eq. (3), for the kinetic parameters obtained by the composite differential method I and $f(\alpha)$ functions for reaction models: SB ($m = 0.62$, $n = 3.22$) and F1.5.

From the parameters of this straight line, the kinetic parameters were evaluated obtaining, $E_a = 109.4 \pm 0.4\,\mathrm{kJ\,mol^{-1}}$, $\ln A = 17.68$ (A in $\mathrm{min^{-1}}$); ($r = -0.9942$). The values of kinetic parameters calculated by composite differential method I are in disagreement with values of kinetic parameters evaluated from Kissinger (model-free) method (Table 3). Namely, the composite kinetic method is a more sensitive on drastically change in the rate-limiting step of the considered reaction, for difference from the kinetic methods which uses the peak temperature value (T_p). In the case of model-free peak methods, T_p represents the peak temperature at different heating rates, and the extent of conversion related to the peak is known to change with the heating rate [63]. Also, compared to the isoconversional methods (like as Friedman method), the peak methods have a limitation because it produces only a single value of E_a for the whole process. As a result, the obtained value is sound only if there is no variation of $E_{a,\alpha}$ with α throughout the process. Unfortunately, such variations are quite typical and the model-free peak methods are not capable of detecting them. Therefore, the E_a values obtained by the model-free peak methods should generally be treated with extreme caution, unless an isoconversional method has demonstrated $E_{a,\alpha}$ be independent of α.

Because of the these facts, we can conclude that the values of kinetic parameters obtained by the Kissinger (model-free) peak method are less accurate than values of kinetic parameters calculated from the composite method.

Fig. 7 shows the comparison of experimental and simulated reaction rate versus extent of conversion at heating rates of $\beta = 5\,^{\circ}\mathrm{C\,min^{-1}}$ and $\beta = 20\,^{\circ}\mathrm{C\,min^{-1}}$, for the second and third reaction stage. For reaction rate calculation (Eq. (3)), the values of kinetic parameters obtained by the composite method were used.

Fig. 7 demonstrates that the above established kinetic parameters reproduces the experimental data excellently, which indicates that the SB(m, n) and F1.5 kinetic models are appropriate for describing the second and third reaction stages, respectively.

In order to confirm the relevance of this study, the obtained values of the apparent activation energy were used for predictions of isothermal bone combustion process. The sole evaluation of $E_{a,\alpha}$ dependence is sufficient to predict the isothermal kinetics from non-isothermal data. In this work, we are applied the so-called "isothermal predictions", which means that the non-isothermal kinetic parameters can be used to simulate the variation of the extent of conversion (α) versus time (t) for a given (constant) temperature (T_{iso}) without knowledge of the reaction model [64–66]. The isothermal predictions of bone combustion process, at four different temperatures ($T_{iso} = 200$, 300, 400 and $450\,^{\circ}\mathrm{C}$) using the kinetic parameters evaluated for $\beta = 2.5\,^{\circ}\mathrm{C\,min^{-1}}$ [65] are presented in Fig. 8. The shapes of the isothermal conversion curves at lower temperatures (200–300 °C) were similar, whereas became more complex with further temperature increase due to organic phase decomposition (Fig. 8). These results are in a good correlation with non-isothermal experimental TG curves.

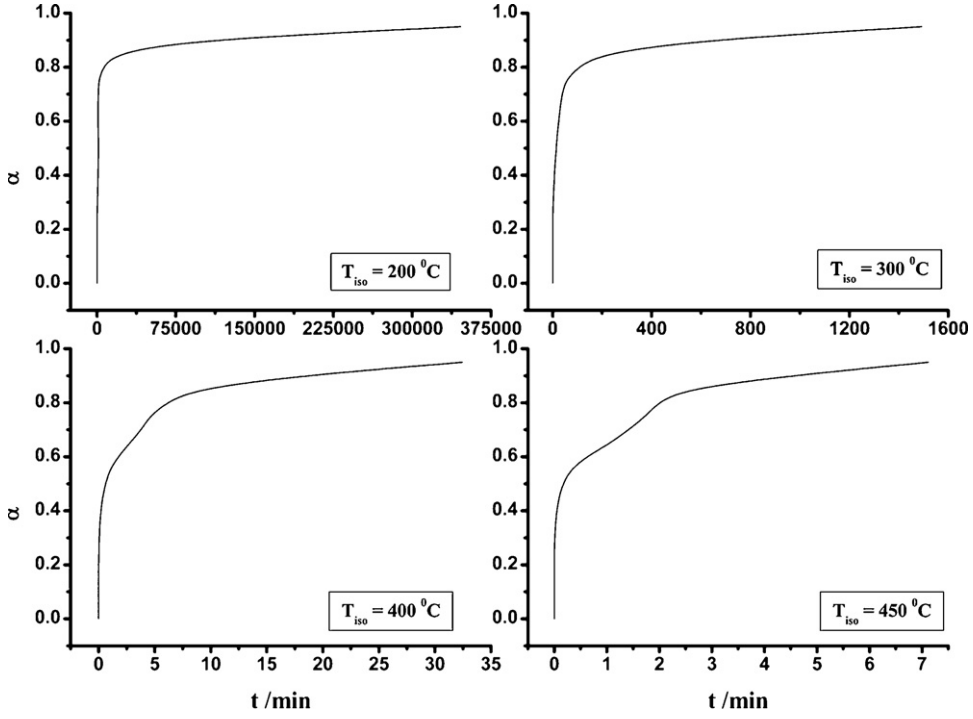

Fig. 8. Predictions of the isothermal combustion kinetics of bovine bone samples at 200, 300, 400 and 450 °C using the kinetic parameters evaluated for $\beta = 2.5\,^{\circ}\mathrm{C\,min^{-1}}$.

5. Discussion

The general discussion of the obtained results for animal bones combustion can be summarized in the following few items:

(A) Water is of significant importance for the living bone, and is one of its major components. Bone water occurs at various locations and in different binding states. From TG–DTA curve (Fig. 1) it can be observed that about 5% of the mass sample represents the most loosely associated water completely evaporates at around 100 °C, which correspond to increasing value of E_a in the range $0.05 \leq \alpha \leq 0.10$ (Fig. 3). This water represents the bulk water which fills the pores of the calcified matrix making up the Haversian and lacuno-canalicular system [67]. Crystal-bound structural water probably occupies vacancies in the imperfect carbonated apatite crystal lattice, providing structural stability by forming hydrogen-bonding bridges between neighboring ions. The presence of this water can explain why the value of E_a abruptly increases up to 212.4 kJ mol^{-1} at $\alpha = 0.15$ (Fig. 3). This sub-step covers the temperature range from 120 to approximately 200 °C. As expected, collagen which has water intimately associated with its structure dehydrated in this reaction stage (stage I, Fig. 3).

The steady increase in E_a up to $\alpha = 0.15$ means that reaction model which contains parallel reactions is probably the most appropriate for the first reaction stage of bone sample [68,69]. This model at least contain two parallel reactions with different apparent activation energies. However, it could be more of them if any of these dehydration processes are influenced by distribution of the apparent activation energies on the precursor, what is the case with dehydration process from mineral phase. The increasing dependence E_a on α for the first stage (stage I, Fig. 3) can be attributed to competing reactions [68]. In our case, we have the competing dehydration reactions from the mineral and organic matrix components of bone. When competing reactions occur, the one with lower apparent activation energy dominates at lower heating rates (under dynamic conditions). If E_a strongly depends on α, it means that the investigated change is complex and cannot be described by a rate equation with only one reaction step (Eq. (3)) [54].

(B) Considering bone collagen, it is presumable that its thermostability is dependent not only on the molecular integrity of collagen itself, but also on the degree of mineralization or on interactions between mineral crystals and collagen molecules.

It can be pointed out that, the active, thermally labile domain in collagen is localized near the C-terminus of the molecule [70,71] the site where cross-links between adjacent collagen molecules are situated [67]. In addition, the backbone of the protein starts to break into fragments [72] between 200 and 350 °C, perhaps after 225 °C (for conversion value at $\alpha = 0.20$) when the DTA exothermic peak begins to increase and when the mass loss slope in TG plot is larger (Fig. 1). This situation corresponds to the degradation stage of organic matrix in the range $0.20 \leq \alpha \leq 0.75$ (stage II, Fig. 3). It was shown, that the bone samples with low organic content, when heated in air, liberated the carbon dioxide in the temperature range 300 °C $\leq T \leq$ 500 °C, i.e. more precisely at $T = 349$ °C [23]. This temperature corresponds to transition region between stages II and III in Fig. 3 at about $\alpha \approx 0.70$–0.75. We can observe in Fig. 3 a continuous decrease in E_a values in the α range $0.35 \leq \alpha \leq 0.65$, which indicates a further degradation of organic phase and separation of smaller side chains from the carbon backbone of molecule. It can be pointed out, that the mineral in bone is located mainly between collagen fibers. Only a small amount of hydroxyapatite crystallites is located in the gap zones [73] between successive tropocollagen molecules [74]. However, mineral additionally stabilizes cross-linked collagen in bone. In our previous paper, the higher mineralized structures which have lower organic content were detected [44]. From these facts, we can explain the relatively high value of E_a at the start of degradation stage of organic phase ($E_a = 139.4$ kJ mol^{-1}) (Fig. 3).

From the previously obtained results, we show that the autocatalytic two-parameter Šesták–Berggren (SB) model for $f(\alpha) = \alpha^{0.62}(1-\alpha)^{3.22}$ can best describe the second reaction stage. The kinetic parameters, m and n define the relative contributions of the acceleratory and decay ("termination") regions of considered process. In SB model, the parameter m is related to the growth dimensionality or branching ratio, while parameter n represents the reaction order. In this mechanism, the reaction rate is accelerated by the intermediate degradation products. Namely, the auto-catalyzed systems are characterized by the formation of some intermediate species which significantly accelerates the reaction. The increasing value of the kinetic exponent m indicates a more important role of the degradation products on the overall kinetics. It seems that a higher value of the kinetic exponent $n > 1$ means increasing complexity. The branching effect can be attributed to the role of the hydroxyapatite crystals as fracture centers [73]. The absence of these fracture centers (which involves the higher thermal stability of collagen) is characteristic of the non-mineralized collagen tissue. For our bone sample we have the opposite case, which can be seen from XRD data [44]. The existence of fracture centers causes the lower number of collagen cross-links, which probably has for a consequence the acceleration of degradation process and contribute in decreasing of E_a values (stage II, Fig. 3).

However, the temptation to equate parameters m and n with a definite collagen degradation mechanism should be avoided, and too much physical significance should not be attached to the numerical values of what is essentially a phenomenological convenience. In particular, this warning applies to processes exhibiting a complex behavior. Therefore, it seems that meaningful conclusions concerning the real mechanism of the process should always be based on other types of complementary evidence, including microscopic observations, mass spectroscopy (MS) together with all other relevant information.

(C) The interpretation of the DTA curve must be related to the way in which the sample was prepared. It has been stated by Nielsen-Marsh et al. [75] that bone shows different thermal behavior if it is ground or studied in larger pieces and this affects the shape of the DTA curve.

In our analysis the particle sizes of the bone samples are higher than 44 μm (45–200 μm) so that the degradation and combustion processes happen as two separated single thermal transformation. If the particle sizes of the samples are less than 44 μm, the degradation and combustion processes of collagen occurs as a single thermal tranformation [75]. In that case, they cannot be distinguished one from another at a specific temperature because both processes contribute simultaneously to the exothermic peak [75]. In Fig. 1, on the presented DTA curves, we can observed the second exothermic peak, which is clearly separated from the first (degradation) exothermic peak. The second exothermic peak can be attributed to the combustion process of collagen in the temperature range 350 °C $\leq T \leq$ 600 °C (which corresponds to $\alpha = 0.75$–0.95 for stage III (Fig. 3)).

The third (III) reaction stage of bone sample was best described by an n-th reaction order model ($f(\alpha) = (1-\alpha)^n$) with $n = 1.5$. This reaction model can be evaluated from the model of Šesták and Berggren for $m = 0$. If $n = 1.5$ and $m = 0$, it has the limit of a fractional order reaction [76,31]. The calculated value of n for the combustion stage (for $n = 1.5$) is almost half the value than corresponding n value calculated for the degradation stage ($n = 3.22$), which indicates that the complexion of combustion stage is upon lower level than degradation stage. It can be noted that the reaction order and the Šesták–Berggren models (with $m = 0$) can lead to very different values, while this was not the case with a real single reaction order mechanism. The complexity of the mechanism can only be deduced from the variation of the kinetic order n, in the reaction order models, but no additional information on

the mechanism can be obtained. Only the differences between the results obtained with the reaction order and the Šesták–Berggren models, supported by different hypotheses, should indicate that a more complex phenomenon is involved. The Šesták–Berggren (SB) model (with $m \neq 0$), also led to approximately constant values for the pre-exponential factor and various values of the kinetic exponents m and n, and in such a case, the SB model can be used only for the modelling purposes.

The degradation and combustion processes (II and III) are linked consecutively at data point $\alpha = 0.75$ (Fig. 3). This behavior can be seen in Fig. 4, where branches 2 and 3 corresponds to the degradation and combustion stages, respectively. In addition, because the compensation coefficients corresponding to all the three stages are different (Table 2) one may conclude that three reaction stages cannot be unified by simple kinetic model.

From the results given above, it can be pointed out that the degree of mineralization and the particle size of the investigated bone samples, can strongly influence the analytical form of the function of reaction mechanism ($f(\alpha)$) for degradation and combustion stage.

The results obtained from isothermal predictions of bone combustion process can have a potential application in various fields of material science and technology where the relationship between temperatures of bone combustion and corresponding reaction times are useful. For example: comparison of different bone samples, production of biogenic hydroxyapatite, production of bone-derived sorbents for environmental applications, etc.

6. Conclusions

In this study, TG–DTA techniques were applied for kinetic analysis of the non-isothermal combustion process of animal bone samples. Different computation methods for the determination of kinetic parameters (A, E_a) were used. It was found that the investigated combustion process of bone samples is a complex, and occurred through three reaction stages (designated as stages I, II and III).

The first stage was described by reaction model, which contains two competing reactions with different values of the apparent activation energy. The autocatalytic two-parameter Šesták–Berggren (SB) model for the mechanism function in the form $f(\alpha) = \alpha^{0.62}(1-\alpha)^{3.22}$ best described the second reaction stage. The second stage represented the degradation process of organic components (mainly collagen), which exhibits an autocatalytic branching effect ($m = 0.62$) with increasing complexity ($n = 3.22$).

From the interpretation of the TG–DTA curves, the third reaction stage was attributed to the organic phase combustion process. This stage was best described by an n-th reaction order model with $n = 1.5$ ($f(\alpha) = (1-\alpha)^{1.5}$). The calculated value of n for the combustion stage ($n = 1.5$) was almost half the value than corresponding n value calculated for the degradation stage ($n = 3.22$), which indicates that the complexion of combustion stage is on a lower level than the degradation stage, probably arises from the bond strength point of view.

The values of kinetic parameters calculated by the composite differential method I were in good agreement with values of kinetic parameters obtained by differential isoconversional (Friedman's) method, for the second reaction stage of considered bone samples. The appearance of compensation effect, clearly showed the existence of three characteristic branches attributed to the dehydration, degradation and combustion processes, respectively.

The isothermal predictions of bone combustion process, at four different temperatures (T_{iso} = 200, 300, 400 and 450 °C) were presented in this paper. It was concluded that the shapes of the isothermal conversion curves at lower temperatures (200–300 °C) were similar, whereas became more complex with further temperature increase due to organic phase decomposition.

Acknowledgment

This study was partially supported by the Ministry of Science and Development of Serbia, under the following Project 142025.

References

[1] M.J. Olszta, X. Cheng, S.S. Jee, R. Kumar, Y.-Y. Kim, M.J. Kaufman, E.P. Douglas, L.B. Gower, Mater. Sci. Eng. Rep. 58 (2007) 77–116.
[2] A.K. Bajpai, R. Singh, Polym. Int. 56 (2007) 557–568.
[3] G.S. Johnson, M.R. Mucalo, M.A. Lorier, J. Mater. Sci.: Mater. Med. 11 (2000) 427–441.
[4] G.S. Johnson, M.R. Mucalo, M.A. Lorier, U. Gieland, H. Mucha, J. Mater. Sci.: Mater. Med. 11 (2000) 725–741.
[5] I.A. Anderson, M.R. Mucalo, G.S. Johnson, M.A. Lorier, J. Mater. Sci.: Mater. Med. 11 (2000) 743–749.
[6] G. Heimke, Adv. Mater. 1 (1989) 122–124.
[7] S. Hodgson, L. Thomas, E. Fattore, P.M. Lind, T. Alfren, L. Hellström, H. Håkansson, G. Carubelli, R. Fanelli, L. Jarup, Environ. Health Perspect. 116 (2008) 1162–1166.
[8] S.-B. Chen, Y.-G. Zhu, Y.-B. Ma, G. McKay, Environ. Pollut. 139 (2006) 433–439.
[9] M. Coutand, M. Cyr, E. Deydier, R. Guilet, P. Clastres, J. Hazard. Mater. 150 (2008) 522–532.
[10] M. Bengisu, Scientometrics 58 (2003) 473–487.
[11] D. Marshall, M.P. Helfrich, R.M. Aspden, Scanning electron microscopy of bone, in: M.H. Helfrich, S.H. Ralston (Eds.), Bone Research Protocols, Methods in Molecular Medicine, 80, 2003, pp. 311–320.
[12] V. Alunni-Perret, M. Muller-Bolla, J. Laugier, L. Lupi-Pgurier, M. Bertrand, P. Staccini, M. Bolla, G. Quatrehomme, J. Forensic Sci. 50 (2005) 1–6.
[13] C.N.G. Trueman, A.K. Behrensmeyer, N. Tuross, S. Weiner, J. Archaeol. Sci. 31 (2004) 721–739.
[14] G.J. Royle, R.D. Speller, Phys. Med. Biol. 40 (1995) 1487–1498.
[15] M. Germine, J.R. Parsons, J. Biomed. Mater. Res. 22 (1988) 55–67.
[16] A. Bartsiokas, A.P. Middleton, J. Archaeol. Sci. 19 (1992) 63–72.
[17] S. Gourion-Arsiquaud, P.A. West, A.L. Boskey, Methods Mol. Biol. 455 (2008) 293–303.
[18] A. Boskey, N. Pleshko Camacho, Biomaterials 28 (2007) 2465–2478.
[19] D. Faibish, A. Gomes, G. Boivin, I. Binderman, A. Boskey, Bone 36 (2005) 6–12.
[20] E.P. Paschalis, F. Betts, E. DiCarlo, R. Mendelsohn, A.L. Boskey, Calcif. Tissue Int. 61 (1997) 487–492.
[21] E. Cappellini, B. Chiarelli, L. Sineo, A. Casoli, A. Di Gioia, C. Vernesi, M.C. Biella, D. Caramelli, J. Archaeol. Sci. 31 (2004) 603–612.
[22] D.M. Mognonov, T.N. Dorzhieva, L.V. Lbova, I.V. Zvontsov, A.I. Buraev, V.V. Khakhinov, Russ. J. Appl. Chem. 75 (2002) 504–506.
[23] L.D. Mkukuma, J.M.S. Skakle, I.R. Gibson, C.T. Imrie, R.M. Aspden, D.W.L. Hukins, Calcif. Tissue Int. 75 (2004) 321–328.
[24] A. Bigi, G. Cojazzi, S. Panzavolta, A. Ripamonti, N. Roveri, M. Romanello, N.K. Suarez, L. Moro, J. Inorg. Biochem. 68 (1997) 45–51.
[25] J.J. Lim, J. Biol. Phys. 3 (1975) 111–129.
[26] F. Peters, K. Schwarz, M. Epple, Thermochim. Acta 361 (2000) 131–138.
[27] E.M. Kurian, J. Therm. Anal. Calorim. 35 (1989) 1111–1117.
[28] J.M. Criado, L.A. Pérez-Maqueda, J. Therm. Anal. Calorim. 80 (2005) 27–33.
[29] W.I. Abdel-Fattah, M.M. Selim, Thermochim. Acta 56 (1982) 345–357.
[30] J.A. Conesa, A. Fullana, R. Font, J. Anal. Appl. Pyrol. 70 (2003) 619–630.
[31] M. Ayllón, G. Gea, M.B. Murillo, J.L. Sánchez, J. Arauzo, J. Anal. Appl. Pyrol. 74 (2005) 445–453.
[32] W. De Jong, G. Di Nola, B.C.H. Venneker, H. Spliethaff, M.A. Wójtowicz, Fuel 86 (2007) 2367–2376.
[33] O. Senneca, Fuel 87 (2008) 3262–3270.
[34] J.A. Conesa, A. Fullana, R. Font, Chemosphere 59 (2005) 85–90.
[35] G. Skodras, P. Grammelis, P. Basinas, S. Kaldis, E. Kakaras, G.P. Sakellaropoulos, Fuel Process. Technol. 88 (2007) 787–794.
[36] P.J. Haines, Principles of Thermal Analysis and Calorimetry, The Royal Society of Chemistry, Great Britain, 2002.
[37] H.L. Friedman, Polym. Sci. C 6 (1963) 183–195.
[38] J.H. Flynn, L.A. Wall, J. Res. Nat. Bur. Stand. A: Phys. Chem. 70 (1966) 487–523.
[39] T. Ozawa, Bull. Chem. Soc. Jpn. 38 (1965) 1881–1886.
[40] H.E. Kissinger, Anal. Chem. 29 (1957) 1702–1706.
[41] T. Akahira, T. Sunose, Res. Rep. Chiba Inst. Technol. 16 (1971) 22–31.
[42] J.M. Criado, L.A. Pérez-Maqueda, F.J. Gotor, J. Málek, N. Koga, J. Therm. Anal. Calorim. 72 (2003) 901–906.
[43] F.J. Gotor, J.M. Criado, J. Málek, N. Koga, J. Phys. Chem. A 104 (2000) 10777–10782.
[44] S. Dimović, I. Smičiklas, I. Plećaš, D. Antonović, M. Mitrić, J. Hazard. Mater. 164 (2009) 279–287.
[45] S. Vyazovkin, N. Sbirrazzuoli, Macromol. Rapid Commun. 27 (2006) 1515–1532.
[46] J.H. Flynn, Thermochim. Acta 300 (1997) 83–92.
[47] M.J. Starink, Thermochim. Acta 404 (2003) 163–176.
[48] C.D. Doyle, Anal. Chem. 33 (1961) 77–79.
[49] A.W. Coats, J.P. Redfern, Nature 201 (1964) 68–69.
[50] S. Vyazovkin, C.A. Wight, Annu. Rev. Phys. Chem. 48 (1997) 125–149.
[51] A. Khawam, D.R. Flanagan, J. Phys. Chem. B 110 (2006) 17315–17328.

[52] E. Wilson, A. Awonusi, M.D. Morris, D.H. Kohn, M.M.J. Tecklenburg, L.W. Beck, J. Bone Miner. Res. 20 (2005) 625–634.
[53] L.D. Mkukuma, C.T. Imrie, J.M.S. Skakle, D.W.L. Hukins, R.M. Aspden, Ann. Rheum. Dis. 64 (2005) 222–225.
[54] P. Budrugeac, E. Segal, Int. J. Chem. Kinet. 33 (2001) 564–573.
[55] M.A. Fernández-Seara, S.L. Wehrli, F.W. Wehrli, Biophys. J. 82 (2002) 522–529.
[56] V.V. Turov, V.M. Gun'ko, V.I. Zarko, R. Leboda, M. Jablonski, M. Gorzelak, E. Jagiello-Wojtowicz, Colloid Surface B: Biointerfaces 48 (2006) 167–175.
[57] A. Techawiboonwong, H.K. Song, M.B. Leonard, F.W. Wehrli, Radiology 248 (2008) 824–833.
[58] C.A. Miles, A.J. Bailey, J. Chem. Sci. 111 (2008) 71–80.
[59] T.I. Ivanova, O.V. Frank-Kamenetskaya, A.B. Kol'tsov, V.L. Ugolkov, J. Solid State Chem. 160 (2001) 340–349.
[60] K. Matsunaga, A. Kuwabara, Phys. Rev. B 75 (2007) 1–9.
[61] S. Vyazovkin, N. Sbirrazzuoli, Macromol. Chem. Phys. 200 (1999) 2294–2303.
[62] J. Šesták, G. Berggren, Thermochim. Acta 3 (1971) 1–12.
[63] N. Sbirrazzuoli, Y. Girault, L. Elégant, Thermochim. Acta 293 (1997) 25–37.
[64] S. Vyazovkin, C.A. Wight, Thermochim. Acta 340–341 (1999) 53–68.
[65] N. Sbirrazzuoli, Macromol. Chem. Phys. 208 (2007) 1592–1597.
[66] D. Zhou, E.A. Schmitt, G.G. Zhang, D. Law, S. Vyazovkin, C.A. Wight, D.J.W. Grant, J. Pharm. Sci. 92 (2003) 1779–1792.
[67] E. Garner, R. Lakes, T. Lee, C. Swan, R. Brand, J. Biomech. Eng. 122 (2000) 166–172.
[68] S.V. Vyazovkin, A.I. Lesnikovich, Thermochim. Acta 165 (1990) 273–280.
[69] S. Vyazovkin, Int. J. Chem. Kinet. 28 (1996) 95–101.
[70] L. Knott, A.J. Bailey, Bone 22 (1998) 181–187.
[71] C.A. Miles, T.V. Burjanadze, A.J. Bailey, J. Mol. Biol. 245 (1995) 437–446.
[72] L.F. Lozano, M.A. Peña-Rico, A. Heredia, J. Ocotlán-Flores, A. Gómez-Cortés, R. Velázquez, I.A. Belío, L. Bucio, J. Mater. Sci. 38 (2003) 4777–4782.
[73] H. Oxlund, L. Sekilde, G. Rtoft, Bone 19 (1996) 479–484.
[74] S. Lees, K. Prostak, Connect. Tissue Res. 18 (1988) 41–54.
[75] C.M. Nielsen-Marsh, R.E.M. Hedges, T. Mann, M.J. Collins, Thermochim. Acta 365 (2000) 129–139.
[76] R. Zakrzewski, Elec. J. Polish Agric. Univ. 6 (2003) 1–12.